scientific reports

Check for updates

OPEN

Transcriptomic and electrophysiological alterations underlying phenotypic variability in *SCN1A*-associated febrile seizures

Stefania Scalise[1,9], Alessandro Gaeta[2,9], Elio Aprigliano[1], Valeria Lucchino[1], Raffaele Covello[1], Mariagrazia Talarico[3], Barbara Puccio[3], Pietro Hiram Guzzi[3], Pierangelo Veltri[4], Antonio Gambardella[3], Lilian Juliana Lissner[2], Alessandra Morano[5], Pierangelo Cifelli[6], Veronica Alfano[8], Eleonora Palma[2,8], Gerardo Perozziello[1], Gabriele Ruffolo[2,7]✉, Giovanni Cuda[1] & Elvira Immacolata Parrotta[3]

Febrile seizures (FS) are a common childhood neurological condition triggered by fever in children without prior neurological disorders. While generally benign, some individuals, particularly those with complex FS or genetic predispositions, may develop epilepsy or other neurological comorbidities. The mechanisms underlying this transition remain unclear. Mutations in *SCN1A*, encoding the $Na_V1.1$ sodium channel α-subunit, have been linked to several epilepsy syndromes associated with FS. This study examines phenotypic variability in individuals carrying the same *SCN1A* c.434T > C mutation, using induced pluripotent stem cell (iPSC)-derived neurons from two siblings with FS. Despite sharing the mutation, only the older sibling developed temporal lobe epilepsy (TLE). Transcriptomic analysis revealed downregulation of GABAergic pathway genes in both siblings' neurons, aligning with *SCN1A*-associated epilepsy. However, neurons from the sibling with TLE exhibited additional abnormalities, including altered AMPA receptor subunit composition, changes in $GABA_A$ receptor subunits and chloride cotransporters expression, and reduced brain-derived neurotrophic factor (BDNF) levels, indicative of developmental immaturity. Voltage-clamp recordings confirmed impaired GABAergic and AMPA receptor-mediated synaptic activity. These findings suggest that combined GABAergic dysfunction, aberrant AMPA receptor composition, and reduced BDNF signaling contribute to the more severe phenotype and increased epilepsy susceptibility.

Keywords Febrile seizure, Mesial temporal lobe epilepsy, Induced pluripotent stem cell-derived neurons, Voltage-gated sodium channel $Na_V1.1$, *SCN1A*, GABAergic dysfunction, Voltage-clamp recordings

Febrile seizures (FS) are the most common neurological disorder in childhood, characterized by fever-induced seizures in children without a history of afebrile seizures or underlying neurological conditions[1]. While generally benign, a subset of individuals, particularly those with complex FS[2] or a genetic predisposition[3,4] is at increased risk of developing epilepsy. Mutations in the *SCN1A* gene, encoding the α-subunit of the $Na_V1.1$ voltage-gated sodium channel (VGSC), are implicated in a spectrum of FS-related epileptic disorders, including Dravet syndrome[5], generalized epilepsy with febrile seizures plus (GEFS +)[6], and simple febrile seizures[7]. However, phenotypic severity can vary significantly among individuals with identical *SCN1A* mutations, likely due to the influence of genetic background[7,8].

To investigate the molecular mechanisms underlying this phenotypic variability, we conducted whole-transcriptome analysis on induced pluripotent stem cell (iPSC)-derived neurons from two siblings with autosomal dominant FS. Fourteen family members are affected, all carrying the c.434 T > C missense mutation

[1]Department of Experimental and Clinical Medicine, Magna Graecia University of Catanzaro, Catanzaro, Italy. [2]Department of Physiology and Pharmacology, Sapienza University of Rome, Rome, Italy. [3]Department of Medical and Surgical Sciences, Magna Graecia University of Catanzaro, Catanzaro, Italy. [4]Department of Informatics, Modeling, Electronics and Systems, University of Calabria, Rende, Italy. [5]Department of Human Neurosciences, Sapienza University, Rome, Italy. [6]Department of Applied Clinical and Biotechnological Sciences, University of L'Aquila, L'Aquila, Italy. [7]IRCCS San Raffaele Cassino, Cassino, Italy. [8]IRCCS San Raffaele Roma, Rome, Italy. [9]Stefania Scalise and Alessandro Gaeta contributed equally to this work ✉email: gabriele.ruffolo@uniroma1.it

in *SCN1A*, resulting in a Met145Thr substitution. This loss-of-function variant leads to a 60% reduction in sodium channel current density and a 10 mV positive shift in the activation curve[7]. While both siblings experienced FS until age six, only the older brother developed temporal lobe epilepsy (TLE) at age 13, indicating a more severe phenotype[9]. This phenotypic divergence highlights the complexity of genotype–phenotype interactions, even within families, and underscores the need to explore the molecular pathways mediating these differences. We previously demonstrated that iPSC-derived neurons from the older brother exhibit electrophysiological abnormalities mirroring those observed in his surgically resected hippocampal tissue[10,11], validating the use of iPSC-derived neurons as a disease model. Importantly, the molecular and electrophysiological alterations associated with *SCN1A* mutations extend beyond the VGSCs themselves, impacting GABAergic inhibitory neurotransmission[12,13] and glutamatergic neurotransmission[14,15].

This aligns with the hypothesis that inborn alterations of key pathophysiological mechanisms, even from single-gene point mutations, can have widespread consequences on brain development, leading to variable phenotypes depending on mutation severity, genetic background, and other pathogenic factors[16].

Therefore, this study aims to analyze the transcriptomic, molecular, and electrophysiological profiles of iPSC-derived neurons from the two *SCN1A*-mutated siblings at different time points. Our goal is to define the extent of *SCN1A* dysfunction during development and establish a link between early neuronal maturation events and the later development of pathologies like FS and TLE.

Results

Generation of forebrain neurons from healthy and SCN1A-mutated iPSCs

To investigate the molecular mechanisms underlying the disease, we differentiated forebrain neurons from iPSCs derived from two healthy controls (HC1 and HC2), the patient with the severe phenotype (SEV), and the patient with the mild phenotype (MILD). The number of neurons per cm^2 obtained after differentiation was comparable across the four iPSC lines (Supplementary Fig. S1A). Neurons were analyzed at early (days 15–20) (Fig. 1A) and late (days 35–45) stages of differentiation (Fig. 1B) . The differentiated neurons expressed key neuronal markers, including microtubule-associated protein 2 (MAP2, Fig. 1C), neurofilament heavy chain (NEFH, Fig. 1C), neurofilament light chain (NEFL, Fig. 1D), and tubulin beta-3 class III (TUBB3, Fig. 1E). Differentiation efficiency was assessed by quantifying the percentage of TUBB3-positive nuclei. All iPSC lines exhibited high differentiation potential, with approximately 85–90% of cells expressing TUBB3 at the early stage of differentiation and reaching nearly 100% at the late stage (Fig. 1F). On the other hand, the expression of the

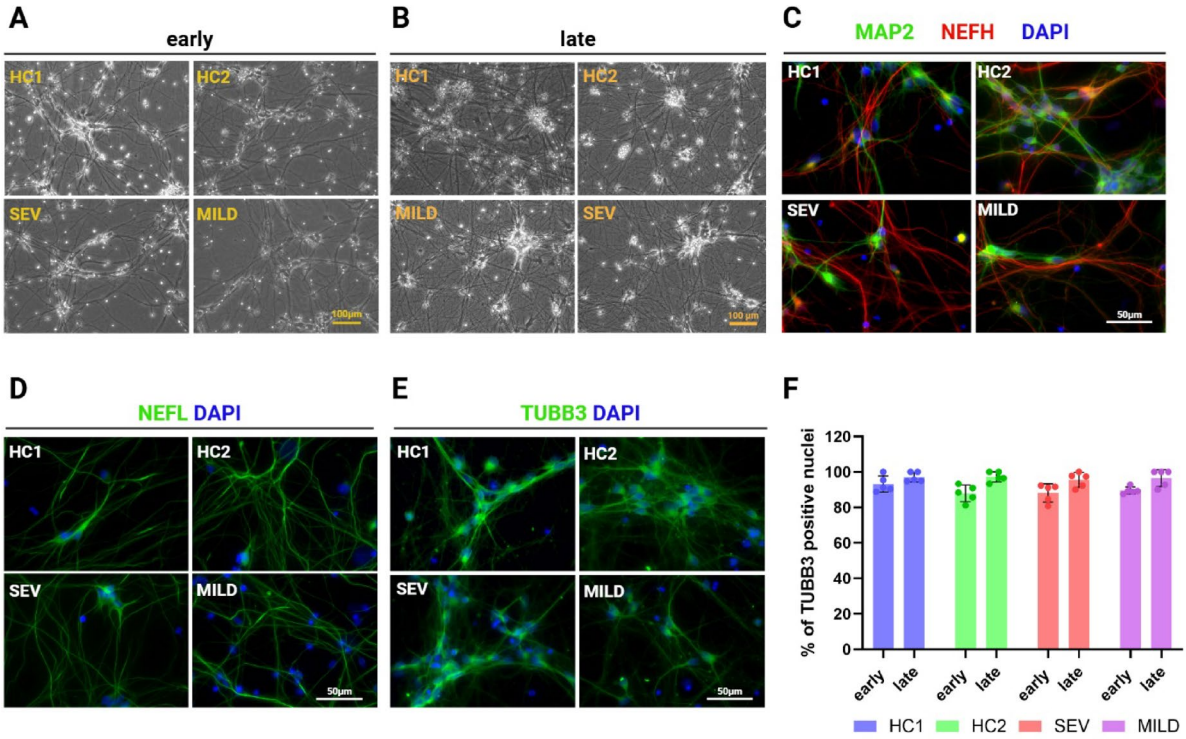

Fig. 1. Generation and characterization of forebrain neurons from iPSC lines. (**A**–**B**) Bright-field images of forebrain neurons differentiated from iPSCs at the early (**A**) and the late (**B**) stages of differentiation. (**C**–**E**) Immunofluorescence staining confirms successful neuronal differentiation, as indicated by the expression of specific neuronal markers: MAP2 and NEFH (**C**), NEFL (**D**), and TUBB3 (**E**). (**F**) Quantification of TUBB3-positive cells demonstrates a high differentiation efficiency (~ 85–90% at the early stage and ~ 100% at the late stage) across all iPSC lines. Data are presented as mean ± S.E.M., with each data point representing an individual analyzed image.

neural stem cell marker PAX6 progressively decreased over time, indicating the gradual loss of undifferentiated progenitors during differentiation (Supplementary Fig. S1B). These results confirm the successful generation of forebrain neurons from both healthy control and patient-derived iPSCs, establishing a robust model for exploring disease-specific cellular and molecular mechanisms.

Transcriptomic analysis reveals impairment of GABAergic transmission in *SCN1A*-mutated neurons

To identify molecular signatures associated with febrile seizures (FS), we analyzed the transcriptomic profiles of iPSC-derived neurons from the two FS patients (SEV and MILD) at early and late differentiation stages, compared to two healthy controls (HC1 and HC2). Gene expression levels (FPKM) showed similar distributions across samples, with peaks around log2(FPKM + 1) and comparable shapes, reflecting the shared neuronal identity (Fig. 2A). This was supported by the FPKM density distribution plot (Fig. 2B). Strong correlations within biological replicates, confirmed by Pearson correlation analysis (Fig. 2C) and principal component analysis (PCA) clustering (Fig. 2D), underscored the reproducibility and robustness of the dataset. Using a

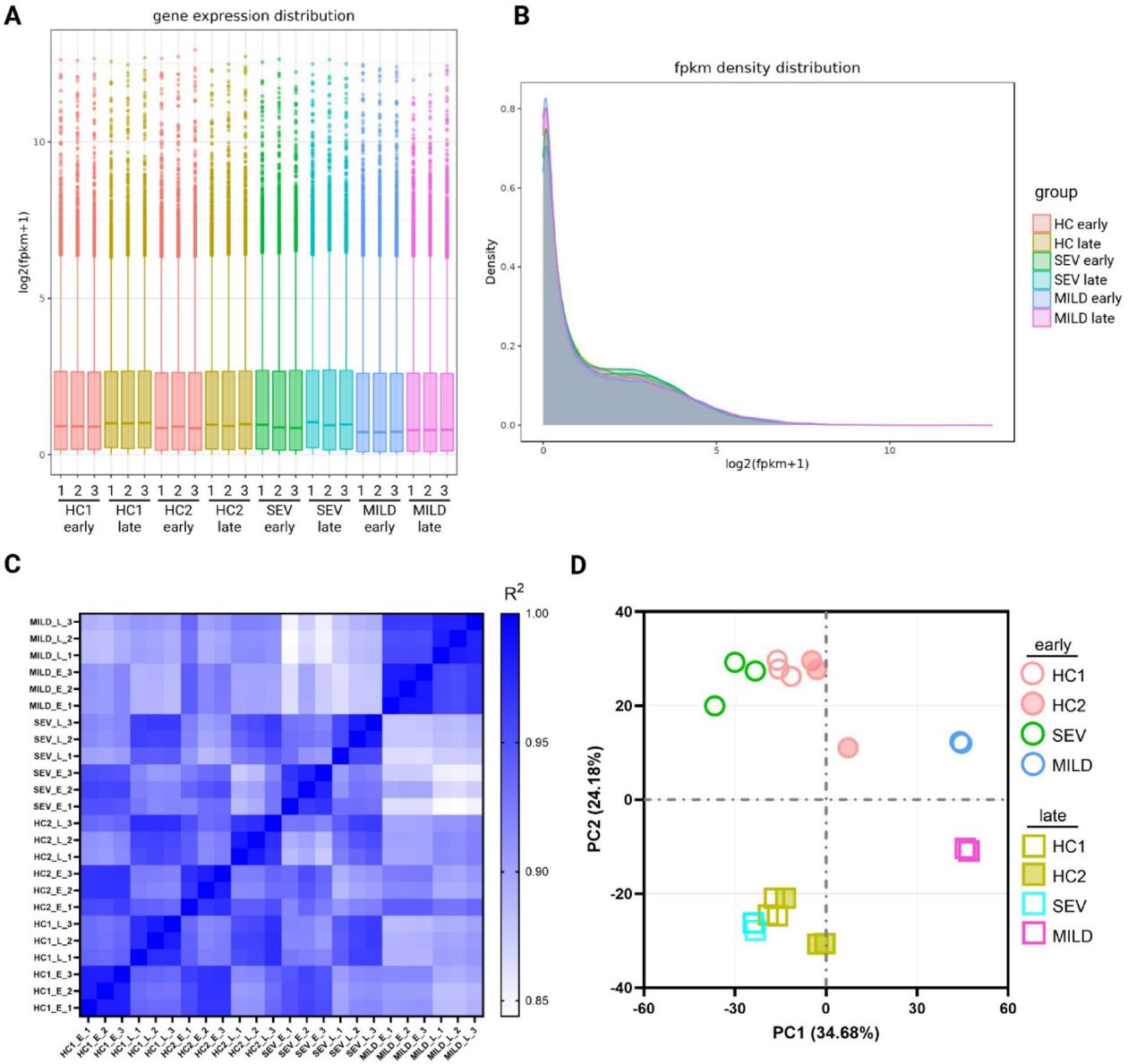

Fig. 2. Analysis of gene expression profiles and consistency across samples. (**A**) Box plot illustrating the distribution of gene expression values (FPKM) across replicates for each sample. (**B**) Density distribution plot depicting the overall gene expression profiles (FPKM values) among all samples. (**C**) Pearson correlation heatmap showing the correlation between samples based on FPKM values. In the sample names, "E" and "L" denote the early and the late stage, respectively. (**D**) Principal component analysis (PCA) of mRNA expression data reveals clustering of biological replicates at both early and late stages of differentiation.

threshold of |Log2 FC| ≥ 1 and an adjusted p-value ≤ 0.05, we identified 698 downregulated and 470 upregulated genes at the early stage in FS patients compared to controls (Fig. 3A, Supplementary Table S1). At the late stage, 623 genes were downregulated and 371 upregulated (Fig. 3B, Supplementary Table S2), indicating distinct gene expression changes across neuronal differentiation. Gene Ontology (GO) enrichment analysis of differentially expressed genes (DEGs) highlighted affected biological processes (BP), molecular functions (MF), and cellular components (CC). Downregulated genes at both stages were enriched for terms related to GABAergic signaling and inhibitory synapse pathways (Fig. 3C, Supplementary Tables S3–S4). Upregulated genes were associated with pathways unrelated to brain-specific functions (Supplementary Tables S5–S6). Gene Set Enrichment Analysis

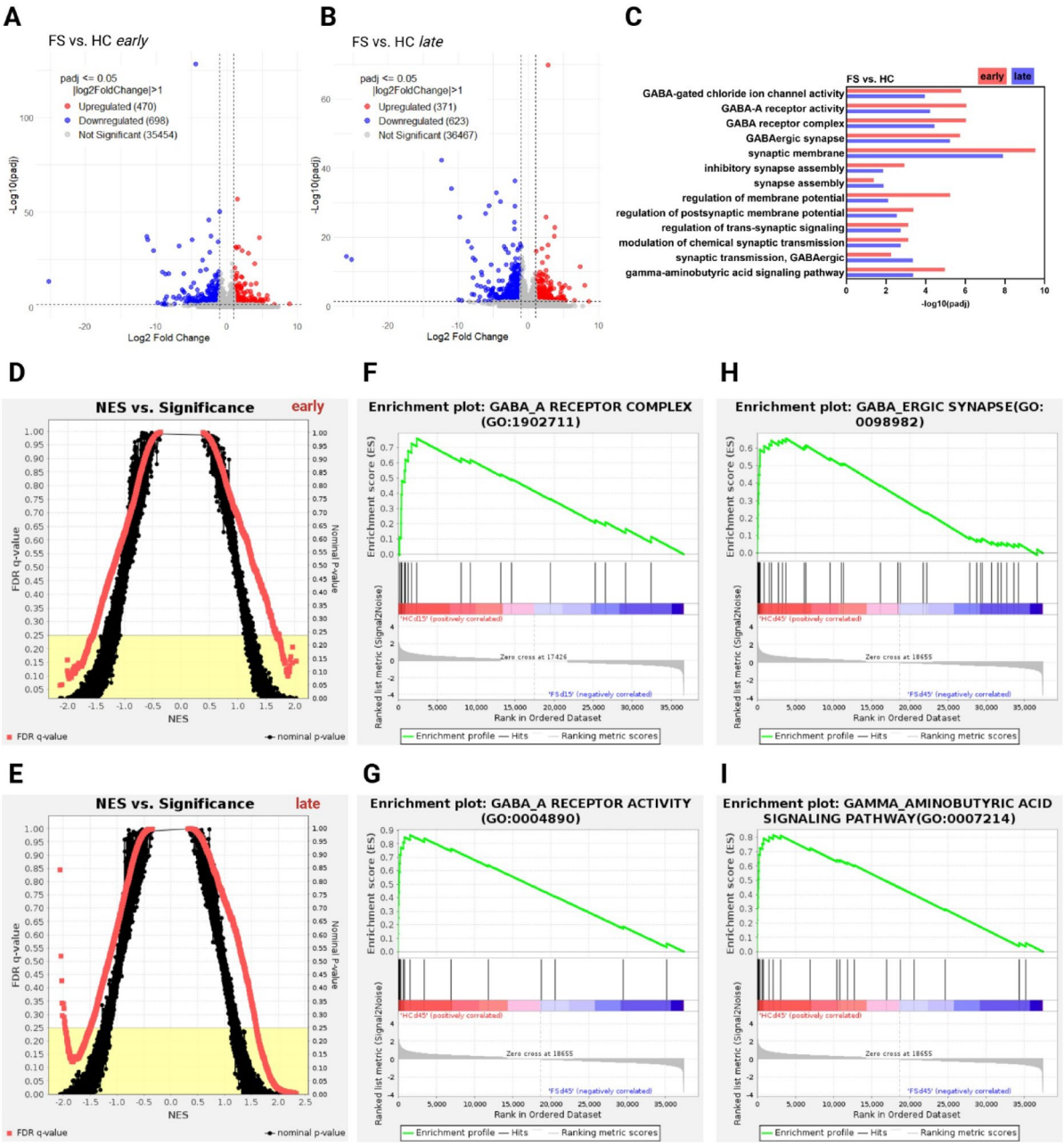

Fig. 3. Transcriptomic analysis revealed altered gene expression in FS neurons. (**A** and **B**) Volcano plots depicting differentially expressed genes (DEGs) between neurons derived from FS patients and HC at the early (**A**) and late (**B**) stages of differentiation. (**C**) Gene Ontology (GO) enrichment analysis of down-regulated DEGs in FS patient-derived neurons compared to HC at both stages of differentiation. (**D** and **E**) Normalized enrichment score (NES) versus significance plot for the early (**D**) and late (**E**) stages of differentiation. The red squares represent the FDR q-value, while the black dots denote the nominal p-value for each gene set. Gene sets are considered significant if the FDR < 25% (highlighted in the yellow box). (**F**–**I**) Gene set enrichment analysis (GSEA) of GO categories highlights the negative enrichment of $GABA_A$ receptor complex and activity, GABAergic synapse, and GABA signaling pathway in neurons derived from FS patients.

(GSEA) further explored these differential expression patterns (Fig. 3D–E). GSEA revealed significant negative correlations for $GABA_AR$-related pathways in FS patients at both differentiation stages (Fig. 3F–G). Pathways associated with GABAergic synapses and signaling also exhibited negative correlations at the late stage (Fig. 3H–I), consistent with the known disruption of GABAergic inhibition in *SCN1A* loss-of-function mutations[17,18]. To assess whether changes in inhibitory signaling were due to a shift in neuronal subtype composition, we examined the expression of canonical glutamatergic (*SLC17A7*, *SLC17A6*, *GLS*, *GLUD1*, *GLUL*, *GRIN1*, and *GRIN2B*) and GABAergic (*GAD2*, *GABARAP*, *GAD1*, *SLC32A1*, *SLC6A1*, *GABBR2*, *GABARAPL1*, *GABARAPL2*, and *GABBR1*) markers across all samples at both early (Supplementary Fig. S1C) and late (Supplementary Fig. S1D) stages of differentiation. Overall, glutamatergic markers showed slightly higher expression levels than GABAergic markers, indicating a mild predominance of excitatory neurons across the cultures. To evaluate the ratio of excitatory vs. inhibitory neurons at early and late stages of differentiation, we calculated, for each line, the ratio of the sum of normalized read counts of glutamatergic markers to GABAergic markers. This analysis did not reveal significant differences in the glutamatergic/GABAergic ratio between the different subjects (Supplementary Fig. S1E). These findings suggest a comparable neuronal subtype distribution across the different iPSC-derived cultures, indicating that the observed variations are not due to differences in cellular population composition but rather reflect a compromised GABAergic inhibitory transmission in SCN1A variant neurons, providing insight into FS pathophysiology.

Glutamatergic signaling disruption and neuronal immaturity in the severe phenotype

To identify the molecular signature of the severe phenotype (SEV), we compared transcriptomes of SEV versus HC and SEV versus MILD. The SEV versus HC comparison revealed 2,500 DEGs at the early stage (1,483 upregulated, 1017 downregulated) and 1,106 DEGs at the late stage (529 upregulated, 577 downregulated) (Supplementary Fig. S2 A and S2 B, Supplementary Tables S7–S8). The SEV versus MILD comparison showed even more DEGs: 5,700 at the early stage (3,736 upregulated, 1964 downregulated) and 4,981 at the late stage (3,677 upregulated, 1,304 downregulated) (Supplementary Fig. S2 C and S2 D, Supplementary Tables S9–S10). GO enrichment analysis revealed significant enrichment of terms related to synaptic transmission, neurotransmitter activity, calcium and glutamate signaling (BP); synapses, neuronal components, and channels (CC); and ion channel activity (MF) in downregulated genes at the early stage for both SEV versus HC and SEV versus MILD (Fig. 4A). At the late stage, similar synapse-related terms were enriched (Fig. 4B), highlighting synaptic dysfunction in the severe phenotype.

GSEA further highlighted the negative enrichment of glutamatergic transmission pathways in SEV cells at the early stage. In the SEV versus HC comparison, pathways like Glutamate Receptor Signaling Pathway (Normalized Enrichment Score (NES) = −1.849) and Glutamatergic Synapse (NES = −2.028) were negatively correlated with the SEV patient. Similarly, the *Ionotropic Glutamate Receptor Signaling pathway* (NES = −1.782) showed negative enrichment in the SEV *versus* MILD comparison (Fig. 4C). These findings suggest that dysregulation of glutamatergic transmission contributes to the SEV phenotype. To corroborate this, we analyzed the expression of genes encoding AMPA receptor subunits, GluA1 (*GRIA1*) and GluA2 (*GRIA2*), crucial for synaptic plasticity[19]. The expression of these subunits is developmentally regulated, with an increase in GluA2 expression during neuronal maturation[20]. While *GRIA1* expression remained consistent in HC and MILD neurons, SEV neurons showed upregulated *GRIA1* during differentiation (Fig. 4D). In contrast, *GRIA2* expression increased from early to late stages across all cell lines, but SEV neurons had lower *GRIA2* expression (Fig. 4E). A higher *GRIA1*-to-*GRIA2* ratio, indicative of neuronal immaturity[21], was observed in SEV neurons (Fig. 4F). These findings suggest that SEV neurons are characterized by both impaired glutamatergic signaling and developmental immaturity, potentially underlying the severe phenotype.

Developmental immaturity of SEV neurons

To further assess the developmental immaturity of SEV neurons, we analyzed the average expression levels across neurons of all lines used in this study of α (*GABRA1-A6*), β (*GABRB1-B3*), and γ (*GABRG1-G3*) $GABA_AR$ subunits at early and late differentiation stages. Among the α subunits, *GABRA3* exhibited the highest expression at both stages[22] (Supplementary Fig. S3 A). Similarly, *GABRB3* was the most highly expressed β subunit (Supplementary Fig. S3 B), and *GABRG3* and *GABRG2* were the most highly expressed γ subunits (Supplementary Fig. S3 C). These subunits are typically present in immature neurons[23–25], suggesting, together with other features, a persistent immature phenotype even at the late differentiation stage.

While we observed a statistically significant increase in the expression of most $GABA_AR$ subunit genes (except *GABRA3*) from early to late stage, indicating general neuronal maturation (Supplementary Fig. S3 A), comparing *GABRA3* expression (the most highly expressed α subunit) with *GABRA1* (α subunit) and *GABRB2* (β subunit), which are typically expressed later in development[25], revealed significantly higher *GABRA3*/*GABRA1* (Fig. 5A) and *GABRA3*/*GABRB2* (Fig. 5B) ratios in SEV neurons. This suggests greater immaturity in the SEV cell line.

During neuronal development, the activity of chloride transporters *SLC12A2* (NKCC1) and *SLC12A5* (KCC2) modulates $GABA_AR$ function[26]. A high NKCC1/KCC2 ratio is associated with brain immaturity[27]. SEV neurons exhibited significantly higher *SLC12A2* (NKCC1) expression at both stages (Fig. 5C), consistent with our previous findings[10]. Conversely, the *SLC12A5* (KCC2) expression was lower in SEV neurons (Fig. 5D), resulting in a higher NKCC1/KCC2 ratio (Fig. 5E), further supporting the immature phenotype. To validate these transcriptional differences at the protein level, we performed KCC2 immunostaining and quantified KCC2-positive puncta per cell (Fig. 5F). SEV neurons displayed a significantly reduced number of KCC2 puncta compared to HC and MILD neurons (Fig. 5G), confirming that lower mRNA levels of KCC2 correspond to reduced protein expression.

KCC2 transcription is regulated by the early growth response transcription factor *EGR4* [28]. While *EGR4* expression increased during differentiation in MILD and HC neurons, SEV neurons showed comparable levels

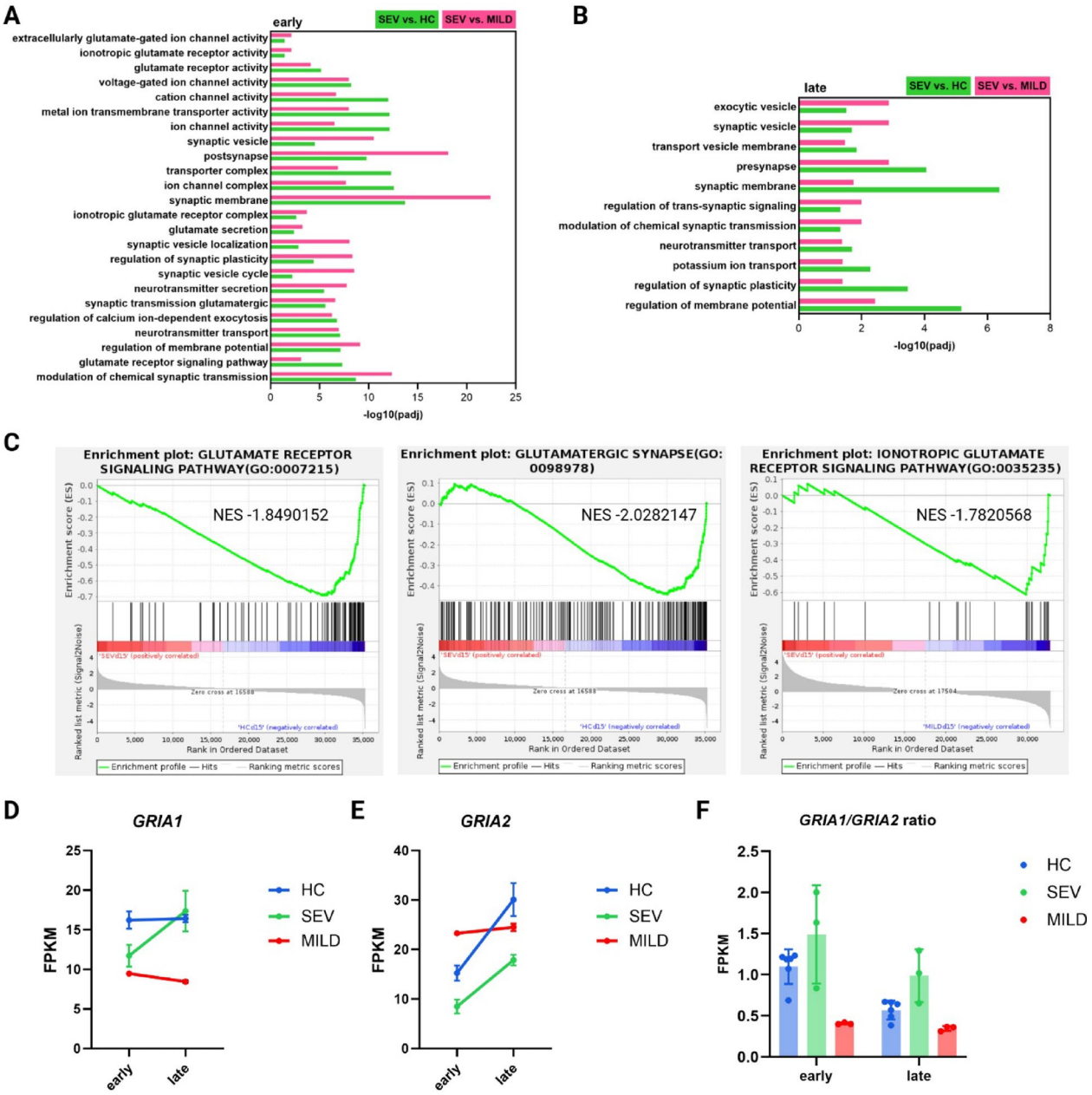

Fig. 4. Impaired glutamatergic signaling and neuronal immaturity in SEV lines. (**A**) GO enrichment analysis of downregulated DEGs at the early stage of differentiation in SEV versus HC and SEV versus MILD comparisons. (**B**) GO enrichment analysis of downregulated DEGs at the late stage of differentiation in SEV versus HC and SEV versus MILD comparisons. (**C**) Gene set enrichment analysis (GSEA) confirms negative enrichment of glutamatergic signaling-related terms in SEV versus HC and SEV versus MILD comparisons. (**D** and **E**) Expression of genes encoding for AMPA receptor subunits GRIA1 and GRIA2 across differentiation stages, showing increased GRIA1 and reduced GRIA2 expression in SEV neurons compared to HC and MILD lines. Data are presented as mean ± S.E.M. of 6 biological replicates for controls and 3 biological replicates for patients. (**F**) *GRIA1/GRIA2* ratio in neurons at early and late stages of differentiation.

at both stages, failing to properly upregulate *EGR4* (Fig. 5H). At the late stage, *EGR4* expression was significantly lower in SEV neurons (Fig. 5H), suggesting a role for reduced *EGR4* in their immaturity. EGR4-dependent KCC2 regulation is modulated by BDNF through the ERK1/2 pathway[28]. GSEA revealed a negative enrichment of the *Neurotrophin Signaling Pathway* in the SEV *versus* MILD comparison at the late stage (NES = -1.2047625) (Fig. 5I). SEV neurons also exhibited significantly lower *BDNF* mRNA levels at both stages (Fig. 5J). At the late stage, *BDNF* expression correlated closely with *EGR4* expression, likely due to increased BDNF receptor (*NTRK2*) expression during neuronal differentiation (Fig. 5K). This suggests that disrupted BDNF signaling may contribute to the developmental immaturity and altered neuronal function in SEV neurons.

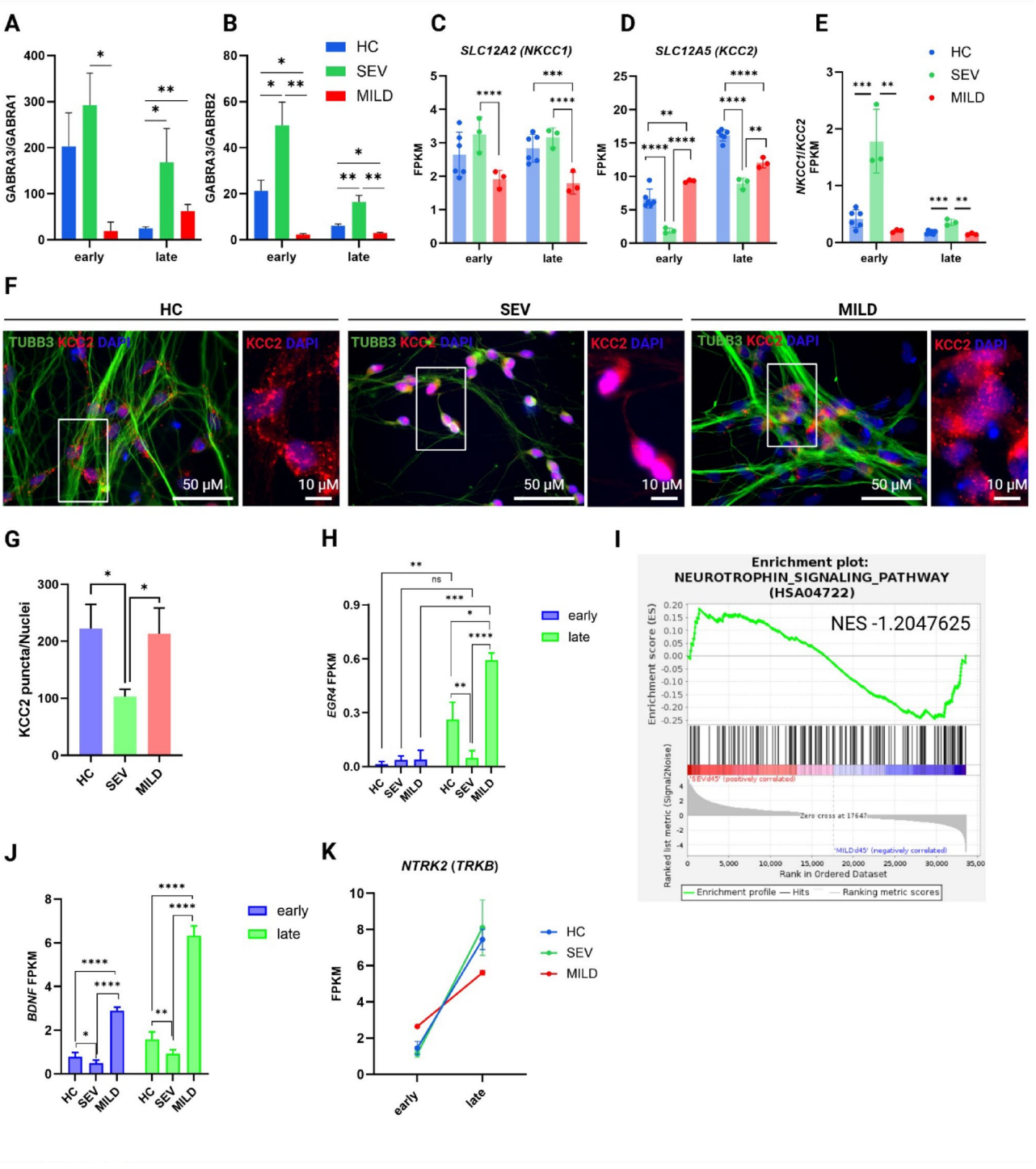

◀**Fig. 5**. Analysis of $GABA_AR$ subunits, chloride channel expression, and BDNF signaling confirm neuronal immaturity in SEV lines. (**A**) Ratios of *GABRA3* to *GABRA1* and (**B**) *GABRA3* to *GABRB2* are significantly higher in SEV neurons, indicating a more immature neuronal state compared to HC and MILD lines. Data are presented as mean ± S.E.M. of FPKM values, with each biological replicate representing the ratio of the indicated subunits. *$p<0.05$, ** $p<0.01$, t-test. (**C**) Expression of chloride channel genes *SLC12A2* (NKCC1) and (D) *SLC12A5* (KCC2) in neurons during differentiation. Data are presented as mean ± S.E.M., with each dot representing a biological replicate. (**E**) The NKCC1/KCC2 ratio is elevated in SEV neurons at both differentiation stages compared to HC and MILD lines. **$p<0.01$, ***$p<0.001$, t-test. (**F**) Representative immunostaining of neurons at the late stage of differentiation, showing KCC2 (red) and TUBB3 (green). *Insets* display a higher magnification, highlighting the localization of KCC2 puncta. (**G**) Quantification of KCC2-positive puncta per cell in HC, SEV, and MILD neurons at the late stage of differentiation. *$p<0.05$, t-test. (**H**) *EGR4* expression during differentiation in HC, SEV, and MILD neurons. (**I**) Negative enrichment of the Neurotrophin Signaling Pathway in SEV versus MILD comparisons at the late stage of differentiation. (**J**) Expression of the *BDNF* gene in HC, SEV, and MILD neurons at both early and late stages of differentiation. (**K**) Expression of *NTRK2* gene (coding for the BDNF receptor) in HC, SEV, and MILD neurons at early and late stages of differentiation.

Electrophysiological characterization of HC and SEV neurons

To analyze the functional characteristics, we used two-electrode voltage clamp recordings on *Xenopus* oocytes injected with neuronal membranes from HC and SEV iPSC-derived neurons. Given the transcriptomic similarity regarding the gene expression of AMPA receptor subunits between MILD and HC, electrophysiological investigations focused on HC and SEV. Therefore, in a series of experiments, we studied AMPA-evoked currents in both HC and SEV phenotypes. Inward currents, evoked by 20 µM AMPA, showed a mean amplitude of − 5.5 ± 1.0 nA (range: − 1.6 to − 9.8 nA; n = 10) in the SEV phenotype and − 21.4 ± 4.7 nA (range: − 2.8 to − 57.5 nA; n = 11) in HC. Given that current amplitude can be influenced by the efficiency of expression in different oocytes or donors, we examined the ratio of 20 µM AMPA current to 500 µM GABA current. At the early stage, the AMPA/GABA current ratio was significantly higher in SEV (567.6 ± 73.6%; n = 10) compared to HC (291.4 ± 29.5%; n = 11; $p = 0.002$, *t-test*) (Fig. 6A). Transcriptomic analysis revealed differential expression of GluA1 and GluA2 mRNA in SEV compared to HC, with reduced *GRIA2* expression. Using the GluA2-lacking receptor blocker IEM 1460 (50 µM), we observed a higher current block rate in SEV (75.1 ± 2.6%; n = 16) compared to HC (63.9 ± 7.2%; n = 10; $p = 0.128$, t-test) (Fig. 6B), suggesting a trend confirming the altered GluA1/GluA2 ratio in FS, consistent with transcriptomic data. Transcriptomic analysis also revealed reduced *GABRG2* (Fig. 7A) and upregulated *GABRB3* and *GABRD* expression (associated with extrasynaptic inhibition[29]) in SEV neurons at the early stage (Fig. 7B-C). Using the γ-less extrasynaptic $GABA_A$Rs selective blocker Zn^{2+} (40 µM), we observed a significantly greater reduction in I_{GABA} amplitude in SEV neurons (− 53.1 ± 3.6%; n = 17) compared to HC (-32.2 ± 4.9%; n = 14) (Fig. 7D), similar to previous findings in control brain samples[30]. This suggests a predominant Zn^{2+}-sensitive, γ-lacking extrasynaptic $GABA_A$ current in SEV neurons, further supporting altered GABAergic signaling.

Discussion

iPSC-derived neuronal models recapitulate aspects of human CNS development, offering valuable insights into how genetic mutations or other stimuli influence disease trajectories[31]. This study examined the transcriptomic and electrophysiological profiles of iPSC-derived neurons from two siblings carrying the same *SCN1A* mutation but exhibiting distinct phenotypes: the younger brother (MILD) presented with febrile seizures (FS) only, while the older brother (SEV) developed mesial temporal lobe epilepsy (mTLE) with hippocampal sclerosis (HS) in adolescence[7,9]. Apart from the alteration due to mTLE, the clinical features, neuroradiological, neurological and psychiatric evaluation were normal in the family members[9]. Our key findings were: (i) both FS patients' neurons showed negative enrichment of genes and pathways associated with GABA signaling; (ii) SEV neurons exhibited altered *GRIA1* and *GRIA2* expression, with increased *GRIA1* and decreased *GRIA2* compared to HC and MILD; (iii) SEV neurons displayed altered $GABA_A$R subunits expression, suggesting persistent immature GABAergic transmission; and (iv) SEV neurons showed impaired electrophysiological properties, with aberrant AMPA- and GABA-mediated responses. Comparing the brothers' neuronal transcriptomes with healthy controls revealed negative enrichment of GABAergic synapse and signaling terms in FS patients across differentiation stages. $GABA_A$Rs, heteropentameric transmembrane ionotropic receptors, predominantly permeable to chloride ions, are ubiquitously expressed in neurons. The early negative enrichment of GABA-related genes suggests impaired GABAergic signaling establishment in FS patients, potentially due to intrinsic defects in GABAergic neurons differentiation[16] or disrupted early synaptic assembly due to *SCN1A* mutations[18,32,33]. These early deficits could impair GABAergic network maturation. This highlights significant GABAergic pathway disruption, consistent with *SCN1A* mutation pathology. *SCN1A* is highly expressed in GABAergic interneurons; loss-of-function mutations impair interneurons excitability, reducing GABA release and inhibitory synaptic activity [34]. These findings support the hypothesis that the FS phenotype from *SCN1A* mutations is also driven by GABAergic dysfunction. During neurodevelopment, GABA and AMPA receptors synergistically regulate neuronal growth, differentiation, and synapse development[35]. AMPARs (GluA1-4 subunits) exhibit temporally regulated functional properties through subunit composition changes[36]. GluA2-lacking receptors have higher calcium permeability. GluA2 expression is low in the immature brain, increasing during development[20]. Our transcriptomic analysis revealed altered glutamatergic signaling in SEV neurons, with increased *GRIA1* (GluA1) and decreased *GRIA2* (GluA2) expression compared to HC and MILD. This higher *GRIA1/GRIA2* ratio suggests neuronal immaturity in SEV cells[21]. Two-electrode voltage clamp recordings revealed a significantly higher AMPA/GABA current ratio in SEV versus HC at early stages, suggesting an imbalance contributing to impaired brain development and neuronal disorders. This is consistent with evidence of complex dysregulation of glutamate receptor subunit genes (e.g., *GRIA1*) and neuronal activity-related genes in epilepsy[37]. The trend toward higher IEM 1460 (GluA2-lacking receptor blocker) inhibition in SEV samples further supports impaired glutamatergic signaling and developmental immaturity. Impaired glutamatergic signaling may also increase brain excitability and seizure susceptibility, enhancing FS occurrence. Complex FS, often associated with mTLE, can lead to *GRIA1* upregulation, contributing to mTLE pathogenesis[38]. We also observed dysregulated $GABA_A$Rs composition in SEV neurons. γ-containing $GABA_A$R are synaptic, mediating fast phasic inhibition[39,40], while δ-containing receptors are extrasynaptic, mediating slow tonic inhibition[41,42]. $GABA_A$R subunit expression is developmentally regulated, with higher α3-, α4-, and α5-containing $GABA_A$Rs and fewer α1-containing receptors observed during embryonic development[23]. Early development sees predominant α2, α3, α5, and β3 subunit mRNAs, gradually replaced by α1, α4, β2, and δ subunit mRNAs in the adult brain. Our analysis of early-stage cells (normalized to α3 expression) showed higher *GABRD* and *GABRB3* expression and reduced *GABRA1* and *GABRG2* expression in SEV neurons. *GABRA1* mutations can cause epilepsy[43] and *GABRG2* is crucial for synaptic receptor formation[44,45] as it stabilizes newly formed synaptic receptors during the neonatal period[46]. We hypothesize that diminished *GABRA1* and *GABRG2* expression in SEV neurons disrupts the balance between phasic and tonic inhibition. Indeed, Zn^{2+} (γ-lacking extrasynaptic $GABA_A$R blocker) reduced I_{GABA} amplitude more in SEV neurons, confirming a predominant Zn^{2}-sensitive, γ-lacking

extrasynaptic $GABA_AR$ composition in SEV. Our results align with evidence that reduced inhibition and excess glutamate activation are associated with generalized epilepsy[47]. This is consistent with our results, which show greater sensitivity to Zn^2-induced blockade of γ-lacking extrasynaptic receptors, suggesting a predominant tonic extrasynaptic component over the phasic synaptic component in SEV neurons. In conclusion, our main purpose was to show that these features can be found in this cellular model of SCN1A mutation-induced disorders, thus validating our model for the study of this disease during neuronal development. Indeed, in future studies, we will aim to test therapeutic strategies that target the pathological alteration described in this study to verify how they can change the abnormal development of iPSC-derived neurons.

Methods

Pathological features and iPSCs generation from the patients with a missense mutation in the SCN1A gene

Induced pluripotent stem cells (iPSCs) were generated from skin fibroblasts of subjects IV-3 and IV-4 from the previously described family pedigree[7,9]. In this study, iPSCs derived from subject IV-3 were labeled as "SEV" and those from subject IV-4 as "MILD". Both individuals harbor a familial missense mutation (c.434 T > C) in exon 3 of the *SCN1A* gene, resulting in the substitution of a conserved methionine with threonine in the S1 segment of domain 1 of the NaV1.1 voltage-gated sodium channel. This mutation is associated with febrile seizures (FS) during childhood; however, the SEV subject also developed mesial temporal lobe epilepsy (mTLE) at age 13. Over time, the SEV phenotype became refractory to anti-epileptic drugs and eventually required lobectomy to control seizures. The iPSC lines derived from these patients were fully characterized previously[48]. For controls, we used the iPSC lines iPSCs-1 and iPSCs-3, previously described[49], here referred to as HC1 and HC2. iPSCs were cultured on Matrigel-coated dishes (Corning, NY, USA) in mTeSR1 medium (StemCell Technologies, Vancouver, BC, Canada) in a humidified incubator at 37 °C and 5% CO_2.

Differentiation of neurons from iPSCs

To differentiate iPSCs into neurons, the cells were first induced to form neural stem cells (NSCs) using Gibco® PSC Neural Induction Medium (Thermo Fisher Scientific, Waltham, MA, USA), following the manufacturer's instructions. The resulting NSCs were seeded at a density of 5×10^4 cells/cm^2 onto dishes coated with Poly-D-Lysine (molecular weight 30,000–70,000) and Laminin (both from Merck, Darmstadt, Germany). Cells were cultured in Neuronal Differentiation Medium (NMDC), supplemented with 1 × B27, 1 × Glutamax, 1 × CultureOne™ Supplement, 200 µM ascorbic acid, and 0.2% Penicillin/Streptomycin (all from Thermo Fisher Scientific). Media changes were performed every three days. To enhance neuronal differentiation, glial cell-derived neurotrophic factor (GDNF) at 10 ng/mL and brain-derived neurotrophic factor (BDNF) at 20 ng/mL (both from PeproTech, London, UK) were added to the NMDC at the time of NSC plating. Following the first medium change, the concentrations of GDNF and BDNF were reduced to 5 ng/mL and 10 ng/mL, respectively. From the second medium change onward, NMDC was supplemented only with BDNF, initially at 5 ng/mL, followed by 2.5 ng/mL for the remainder of the differentiation period. Neurons were harvested after 15–20 days of differentiation as the "early stage" and after 35–45 days as the "late stage" for further analysis. To quantify the absolute number of neurons obtained per cm^2, after 15 days of differentiation, cells were dissociated and counted using CellDrop automated cell counter (DeNovix Inc., Wilmington, DE, USA). The proportion of neurons was estimated by TUJ1 immunostaining and image-based quantification. Neuronal yield per cm^2 was calculated by multiplying total cells/cm^2 by the percentage of $TUJ1^+$ cells.

Library construction for RNA-seq analysis

Total RNA for RNA-Seq analysis was extracted from neurons at early and late differentiation stages from two healthy controls (HC1 and HC2) and two patients (SEV and MILD) using TRIzol reagent (Thermo Fisher Scientific), and mRNA was subsequently isolated from the total RNA using poly-T oligo-attached magnetic beads. After mRNA fragmentation, first-strand cDNA was synthesized using random hexamer primers, followed by second-strand cDNA synthesis. Library quantification was performed using a Qubit fluorometer and real-time PCR, while the size distribution of the libraries was assessed using Bioanalyzer analysis. The quantified libraries were pooled and sequenced on Illumina platforms, ensuring the appropriate concentration and data yield for optimal sequencing performance.

Data quality control, reads mapping, and gene expression quantification

Raw sequencing data in FASTQ format were initially processed using fastp software to ensure high-quality reads for downstream analyses (version v0.23.4; https://github.com/OpenGene/fastp/tree/v0.23.4). During this step, adapter sequences, reads containing poly-N, and low-quality reads were discarded, resulting in clean reads. Quality metrics, including Q20, Q30, and GC content, were calculated for the clean reads. Only high-quality reads were retained for subsequent analysis. Reference genome and gene annotation files were downloaded from genome repositories. The reference genome index was built using Hisat2 v2.0.5[50] and paired-end clean reads were aligned to the reference genome using the same tool. Results of RNA-seq data quality control and alignment to the reference genome are presented in Supplementary Figures S4 -S7 . Gene expression levels were quantified using featureCounts v1.5.0-p3[51], which assigns sequence reads to genomic features. The resulting expression levels were normalized and reported as FPKM (Fragments Per Kilobase of transcript sequence per Million base pairs sequenced), accounting for both sequencing depth and gene length.

Differential expression analysis

Differential expression analysis was performed between FS and HC, SEV and HC, and SEV and MILD groups using the DESeq2 R package (version 1.20.0)[52], with three biological replicates per group. The data from the two

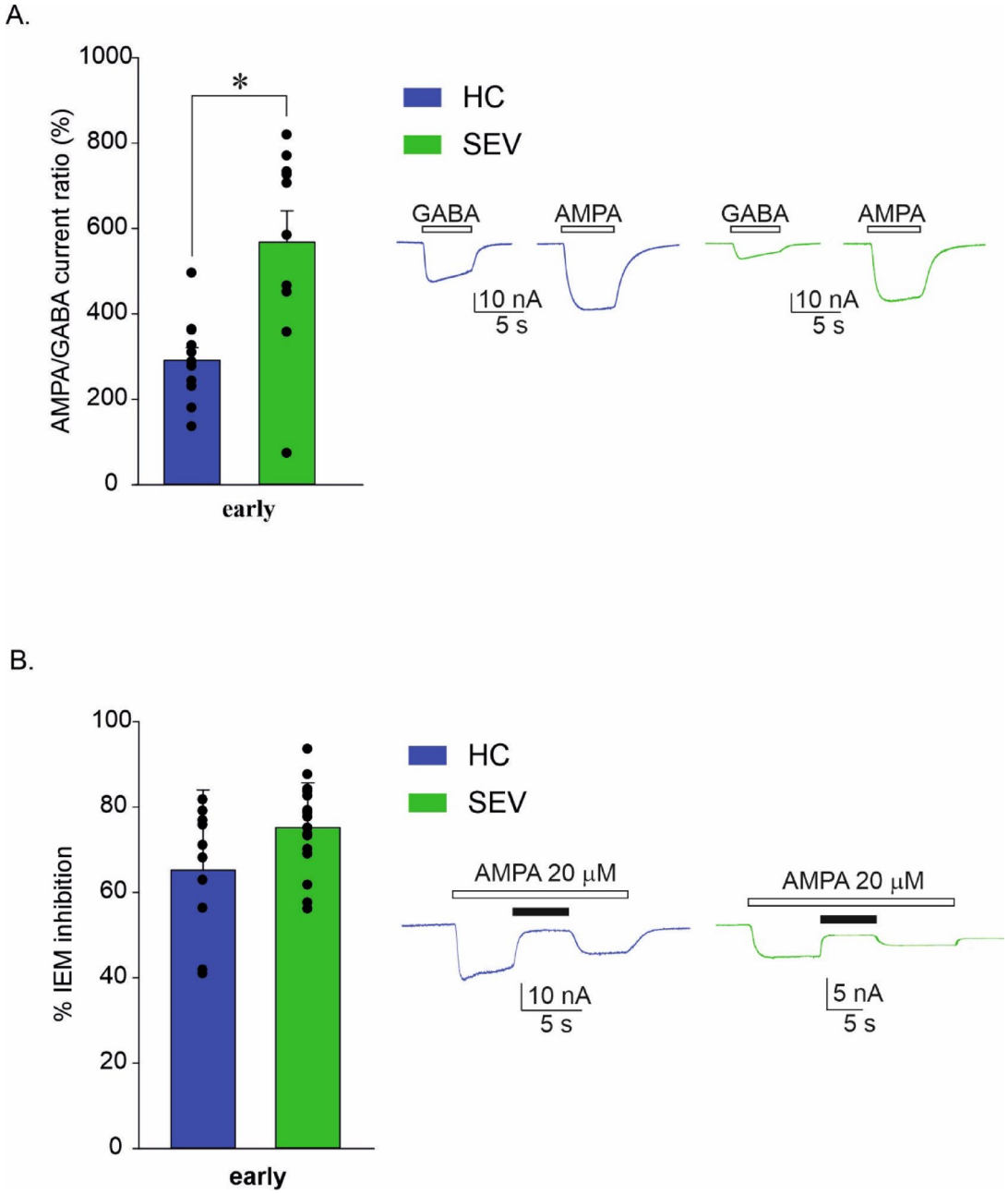

Fig. 6. Analysis of AMPA/GABA current by voltage clamp. (**A**) AMPA/GABA current ratio (expressed as percentage ± S.E.M.) of 20 μM AMPA- and 500 μM GABA-evoked currents at the early stages of differentiation. The AMPA/GABA current ratio was significantly different between the two phenotypes (blue filled bar: 291.4 ± 29.5%, n = 11; versus green filled bar: 567.6 ± 73. 6%, n = 10; $p = 0.002$, *t-test*). The *inset* on the right shows the GABA- and AMPA-evoked current traces. (**B**) AMPA-evoked current (percentage ± S.E.M.) blocked by 50 μM IEM 1460 (a selective blocker for GluA2-lacking receptors) in HC and SEV phenotypes (blue filled bar: 63.9 ± 7.2%; n = 10; vs green filled bar: 75.1 ± 2.6%; n = 16; $p = 0.128$, *t-test*). The *inset* on the right shows AMPA-evoked currents recorded from samples with IEM 1460 application (50 μM, black bar) to block GluA2-lacking AMPAR currents. IEM 1460 inhibition was tested using a holding potential of − 80 mV.

control subjects were combined and analyzed as a single "HC" group (total of six biological replicates), while the data from the two patients (SEV and MILD) were treated as the FS group for the FS versus HC comparison. *P*-values from the comparisons were adjusted for multiple testing using Benjamini and Hochberg's method to control the false discovery rate (FDR). Genes with an adjusted p-value ≤ 0.05 were considered differentially expressed. To further investigate the biological implications of the differentially expressed genes (DEGs), Gene Ontology (GO) enrichment analysis was conducted using the clusterProfiler R package. GO terms with a corrected p-value ≤ 0.05 were considered significantly enriched, providing insights into the biological processes (BP), cellular components (CC), and molecular functions (MF) associated with the DEGs.

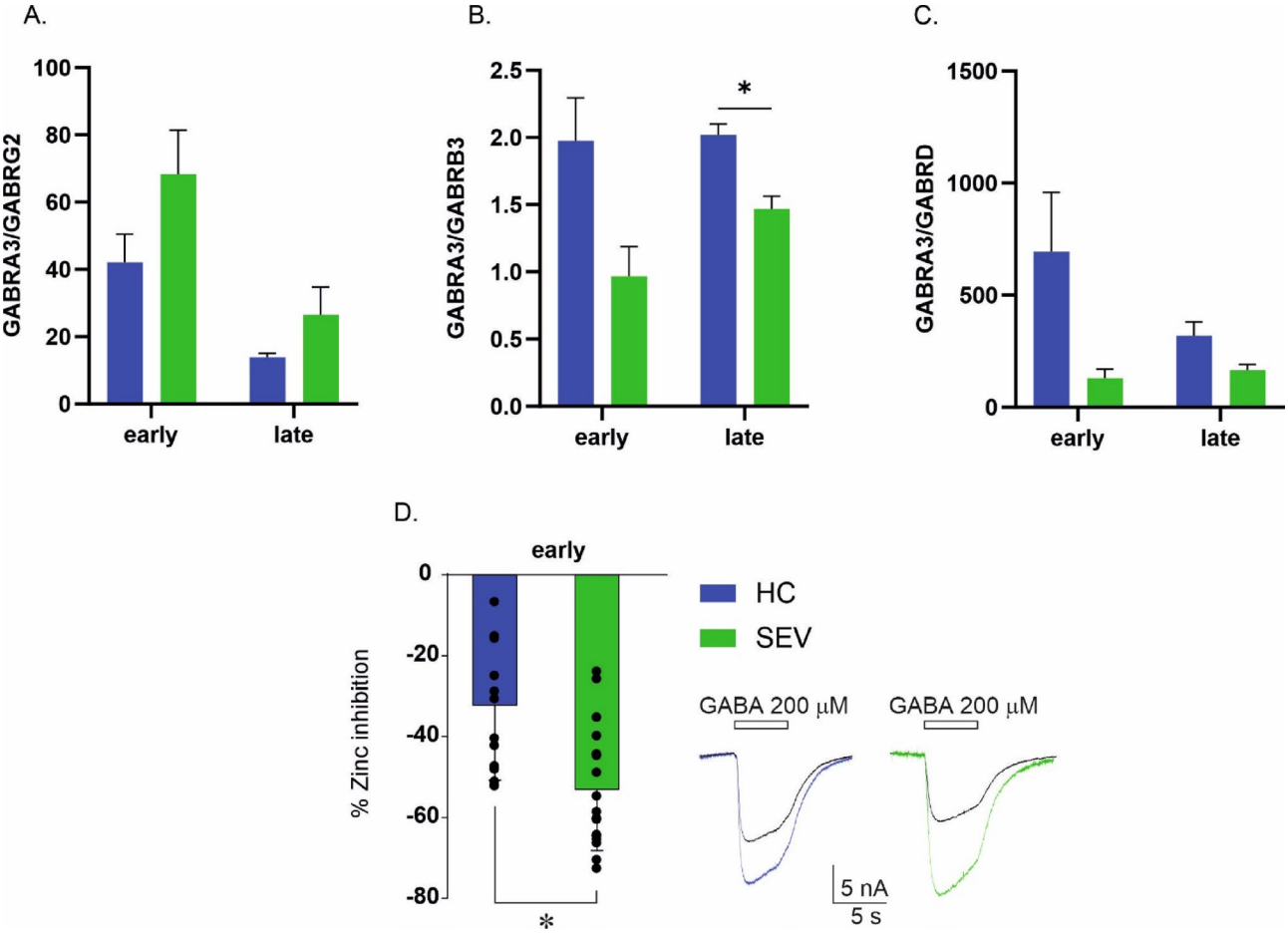

Fig. 7. Zn^{2+} selectively inhibits γ-lacking extrasynaptic $GABA_A$Rs. (**A**) Ratios of *GABRA3* to *GABRG2* (α3/γ2), showing a lower ratio in SEV neurons compared to HC. Conversely, (**B**) the ratios of *GABRA3* to *GABRB3* (α3/β3) and (**C**) *GABRA3* to *GABRD* (α3/δ) are higher in SEV neurons, indicating a more immature state relative to HC lines. (**D**) Percentage decrease in GABA current ± S.E.M. following treatment with 40 μM Zn^{2+} (blue filled bar: − 32.2 ± 4.9%; n = 14; vs green filled bar: − 53.1 ± 3.6%; n = 17; $p = 0.004$, *t-test*). The *inset* on the right shows the 200 μM GABA-evoked current before and after treatment with 40 μM Zn^{2+} (black traces) for both HC and SEV neurons.

Immunofluorescence

Cells were fixed with 3.7% (vol/vol) formaldehyde (Sigma Aldrich, St. Louis, MO, USA) and then blocked for 2 h at room temperature in a solution containing 10% goat serum (Thermo Fisher Scientific) and 0.1% Triton X-100 (Sigma Aldrich) in 1X DPBS with calcium and magnesium (Gibco, Waltham, MA, USA). Following blocking, the cells were incubated overnight at 4 °C with primary antibodies targeting: MAP2 (1:1000, Thermo Fisher Scientific, cat. MA5–12,826), NEFH (1:1000, Abcam, Cambridge, UK, cat. ab8135), NEFL (1:100, Cell Signaling, Danvers, MA, USA, cat. 2837), and TUBB3 (1:250, Thermo Fisher Scientific, cat. 480,011). On the following day, AlexaFluor 488– or 594–conjugated secondary antibodies (1:500, Thermo Fisher Scientific) were applied for 1 h at room temperature. Nuclei were stained with DAPI. For mounting, cover glasses were treated with Dako Fluorescent Mounting Medium (Agilent, Santa Clara, CA, USA). Images were acquired using a Leica DMi8 inverted microscope or a Leica Thunder DMi8 system with LAS X software (v.3.7.4.23463). Immunofluorescence analysis was performed using ImageJ Fiji software (version 1.54p).

Western blot analysis

For total protein extraction, cells were collected in ice-cold phosphate-buffered saline (PBS) and lysed using RIPA buffer (Merck) supplemented with Halt™ Protease and Phosphatase Inhibitor Cocktails (Thermo Fisher Scientific). Protein concentrations were determined using the Bradford assay. Proteins were then denatured by heating at 95 °C for 10 min in Laemmli sample buffer. A total of 20 μg of protein per sample was loaded onto Mini-PROTEAN TGX precast polyacrylamide gels (Bio-Rad, Hercules, CA, USA) and subsequently transferred to a nitrocellulose membrane. Membranes were incubated overnight at 4 °C with primary antibodies: anti-PAX6 (rabbit polyclonal, 1:1,000, #ab5790, Abcam, Cambridge, UK) and anti-TUBB3 (mouse monoclonal, 1:10,000, #480,011, Thermo Fisher Scientific). After washing, membranes were incubated for 1 h at room temperature with horseradish peroxidase (HRP)-conjugated secondary antibodies (anti-rabbit IgG and anti-mouse IgG; Jackson

ImmunoResearch, Cambridge, UK). Protein bands were visualized using Clarity™ Western ECL substrate (Bio-Rad) and imaged with the Alliance™ Q9-Atom system (Uvitec, Cambridge, UK).

Xenopus Laevis oocytes injection and 'two-electrode' voltage clamp recordings

Neuronal membranes were isolated from approximately 7×10^7 neurons differentiated from HC and SEV iPSCs. *Xenopus* laevis oocytes were obtained and injected with the isolated membranes as previously described[53]. The advantage of this approach is recording genuine GABA- and AMPA-evoked currents from the native receptors, at the desired time point, repeatedly over time without compromising their functional properties. Indeed, with our approach we can extract membranes from cells at specific time-points and maintain them at − 80 °C for several months[54]. The two-electrode voltage clamp electrophysiological technique was performed 24–48 h post-injection. Two microelectrodes filled with 3 M KCl were used for recordings. *Xenopus* oocytes were positioned in a 0.1 mL recording chamber, continuously perfused with oocyte Ringer solution (OR: NaCl 82.5 mM; KCl 2.5 mM; $CaCl_2$ 2.5 mM; $MgCl_2$ 1 mM; Hepes 5 mM, pH 7.4, adjusted with NaOH) at room temperature (20–22 °C). Neurotransmitter applications (GABA or AMPA) were controlled by a computer (Biologique RSC-200; Claix, France) using a gravity-driven multi-valve perfusion system (9–10 mL/min) to precisely regulate the timing of each application. The system allowed for the initiation or interruption of solution flow through polyethylene tubes connected to the recording chamber (Harvard Apparatus, Cambridge, MA, USA) via digitally set intervals. GABA (200–500 µM) was applied for 5–7 s to elicit inward GABA-evoked currents (I_{GABA}), while AMPA (20 µM) was applied in the presence of Cyclothiazide (CTZ, 20 µM) to prevent rapid receptor desensitization[10]. The stability of GABA and AMPA currents was assessed by performing two consecutive neurotransmitter applications, separated by a 4-min washout. Only cells with less than a 5% variation in GABA and AMPA current amplitudes between applications were used for subsequent recordings (e.g., testing modulation by IEM 1460 or Zinc) and included in the statistical analysis. In a subset of experiments, the AMPA receptor (AMPAR) voltage-dependent open-channel blocker IEM 1460 (50 µM) was used, which preferentially blocks GluA2-lacking receptors. Additionally, in another experiment, 40 µM $ZnCl_2$ was applied to block Zn^{2+}-sensitive extrasynaptic $GABA_A$Rs[55] .

Ethics approval

All animal experimental protocols involving *Xenopus* laevis frogs, the surgical procedures for oocytes extraction were approved by "Italian Ministry of Health" (authorization no. 427/2020-PR). All the animal procedures followed the recommendations of the ARRIVE guidelines and the methods are reported accordingly. All methods were carried out in accordance with relevant guidelines and regulations.

All the human procedures included in this study were approved by the Ethics Committee of the "Magna Graecia" University of Catanzaro and the Azienda Ospedaliero-Universitaria "Mater Domini" under protocol number AOM92_2020. All experiments were performed following the principles outlined in the Declaration of Helsinki. Informed consent was obtained from all participants before their inclusion in the study.

Data availability

RNA-sequencing data generated in this study are available in the NCBI Gene Expression Omnibus (GEO) and in the supplementary files.

Received: 13 February 2025; Accepted: 25 June 2025
Published online: 10 July 2025

References

1. Camfield, P. & Camfield, C. Incidence, prevalence and aetiology of seizures and epilepsy in children. *Epileptic. Disord.* **17**, 117–123 (2015).
2. Theodore, W. H. et al. Hippocampal atrophy, epilepsy duration, and febrile seizures in patients with partial seizures. *Neurology* **52**, 132–132 (1999).
3. Abou-Khalil, B. et al. Familial genetic predisposition, epilepsy localization and antecedent febrile seizures. *Epilepsy Res.* **73**, 104–110 (2007).
4. Saghazadeh, A., Mastrangelo, M. & Rezaei, N. Genetic background of febrile seizures. *Rev. Neurosci.* **25**, 129–161 (2014).
5. Marini, C. et al. The genetics of Dravet syndrome. *Epilepsia* **52**, 24–29 (2011).
6. Escayg, A. et al. A novel SCN1A mutation associated with generalized epilepsy with febrile seizures plus—and prevalence of variants in patients with epilepsy. *Am. J. Hum. Genet.* **68**, 866–873 (2001).
7. Mantegazza, M. et al. Identification of an Nav 1.1 sodium channel (SCN1A) loss-of-function mutation associated with familial simple febrile seizures. *Proc. Natl. Acad. Sci.* **102**, 18177–18182 (2005).
8. Scheffer, I. E., Zhang, Y.-H., Jansen, F. E. & Dibbens, L. Dravet syndrome or genetic (generalized) epilepsy with febrile seizures plus?. *Brain Dev.* **31**, 394–400 (2009).
9. Colosimo, E. et al. Electroclinical features of a family with simple febrile seizures and temporal lobe epilepsy associated with SCN1A loss-of-function mutation. *Epilepsia* **48**, 1691–1696 (2007).
10. Scalise, S. et al. Human iPSC modeling of genetic febrile seizure reveals aberrant molecular and physiological features underlying an impaired neuronal activity. *Biomedicines* **10**, 1075 (2022).
11. Ruffolo, G. et al. Modulation of GABAergic dysfunction due to *SCN1A* mutation linked to hippocampal sclerosis. *Ann. Clin. Transl. Neurol.* **7**, 1726–1731 (2020).
12. Ruffolo, G. et al. A novel GABAergic dysfunction in human Dravet syndrome. *Epilepsia* **59**, 2106–2117 (2018).
13. Goisis, R. C. et al. GABA tonic currents and glial cells are altered during epileptogenesis in a mouse model of Dravet syndrome. *Front. Cell. Neurosci.* **16**, 919493 (2022).
14. Hameed, M. Q. et al. Depressed glutamate transporter 1 expression in a mouse model of Dravet syndrome. *Ann. Clin. Transl. Neurol.* **10**, 1695–1699 (2023).
15. Studtmann, C., Ladislav, M., Topolski, M. A., Safari, M. & Swanger, S. A. NaV1.1 haploinsufficiency impairs glutamatergic and GABAergic neuron function in the thalamus. *Neurobiol. Dis.* **167**, 105672 (2022).

16. Schuster, J. et al. Epigenetic insights into GABAergic development in Dravet Syndrome iPSC and therapeutic implications. *Elife* **12**, P92599 (2024).
17. Yu, F. H. et al. Reduced sodium current in GABAergic interneurons in a mouse model of severe myoclonic epilepsy in infancy. *Nat. Neurosci.* **9**, 1142–1149 (2006).
18. Ogiwara, I. et al. Nav 1.1 Localizes to Axons of Parvalbumin-Positive Inhibitory Interneurons: A Circuit Basis for Epileptic Seizures in Mice Carrying an Scn1a Gene Mutation. *J. Neurosci.* **27**, 5903–5914 (2007).
19. Diering, G. H. & Huganir, R. L. The AMPA receptor code of synaptic plasticity. *Neuron* **100**, 314–329 (2018).
20. Talos, D. M., Kwiatkowski, D. J., Cordero, K., Black, P. M. & Jensen, F. E. Cell-specific alterations of glutamate receptor expression in tuberous sclerosis complex cortical tubers. *Ann. Neurol.* **63**, 454–465 (2008).
21. Ruffolo, G. et al. Functional aspects of early brain development are preserved in tuberous sclerosis complex (TSC) epileptogenic lesions. *Neurobiol. Dis.* **95**, 93–101 (2016).
22. Succol, F., Fiumelli, H., Benfenati, F., Cancedda, L. & Barberis, A. Intracellular chloride concentration influences the GABAA receptor subunit composition. *Nat. Commun.* **3**, 738 (2012).
23. Fritschy, J., Paysan, J., Enna, A. & Mohler, H. Switch in the expression of rat GABAA-receptor subtypes during postnatal development: an immunohistochemical study. *J. Neurosci.* **14**, 5302–5324 (1994).
24. Cellot, G. & Cherubini, E. Functional role of ambient GABA in refining neuronal circuits early in postnatal development. *Front. Neural Circuits* **7**, 136 (2013).
25. Laurie, D., Wisden, W. & Seeburg, P. The distribution of thirteen GABAA receptor subunit mRNAs in the rat brain. III. Embryonic and Postnatal development. *J. Neurosci.* **12**, 4151–4172 (1992).
26. Kaila, K., Price, T. J., Payne, J. A., Puskarjov, M. & Voipio, J. Cation-chloride cotransporters in neuronal development, plasticity and disease. *Nat. Rev. Neurosci.* **15**, 637–654 (2014).
27. Watanabe, M. & Fukuda, A. Development and regulation of chloride homeostasis in the central nervous system. *Front. Cell. Neurosci.* **9**, 371 (2015).
28. Ludwig, A. et al. Early growth response 4 mediates BDNF induction of potassium chloride cotransporter 2 transcription. *J. Neurosci.* **31**, 644–649 (2011).
29. Farrant, M. & Nusser, Z. Variations on an inhibitory theme: phasic and tonic activation of GABA(A) receptors. *Nat. Rev. Neurosci.* **6**, 215–229 (2005).
30. Palma, E. et al. $GABA_A$ -current rundown of temporal lobe epilepsy is associated with repetitive activation of $GABA_A$ "phasic" receptors. *Proc. Natl. Acad. Sci.* **104**, 20944–20948 (2007).
31. Livesey, M. R. et al. Maturation of AMPAR Composition and the $GABA_A$ R Reversal Potential in hPSC-Derived Cortical Neurons. *J. Neurosci.* **34**, 4070–4075 (2014).
32. Catterall, W. A., Kalume, F. & Oakley, J. C. NaV 1.1 channels and epilepsy: NaV 1.1 channels and epilepsy. *J. Physiol.* **588**, 1849–1859 (2010).
33. Van van Hugte, E. J. H., Schubert, D. & NadifKasri, N. Excitatory/inhibitory balance in epilepsies and neurodevelopmental disorders: Depolarizing γ-aminobutyric acid as a common mechanism. *Epilepsia* **64**, 1975–1990 (2023).
34. Kayabas, M. A. et al. Transition to seizure in focal epilepsy: From SEEG phenomenology to underlying mechanisms. *Epilepsia* **65**, 3619–3630 (2024).
35. Herlenius, E. & Lagercrantz, H. Development of neurotransmitter systems during critical periods. *Exp. Neurol.* **190**, 8–21 (2004).
36. Kumar, S. S., Bacci, A., Kharazia, V. & Huguenard, J. R. A developmental switch of AMPA receptor subunits in neocortical pyramidal neurons. *J. Neurosci.* **22**, 3005–3015 (2002).
37. Pfisterer, U. et al. Identification of epilepsy-associated neuronal subtypes and gene expression underlying epileptogenesis. *Nat. Commun.* **11**, 5038 (2020).
38. Li, Y., Wang, C., Wang, P., Li, X. & Zhou, L. Effects of febrile seizures in mesial temporal lobe epilepsy with hippocampal sclerosis on gene expression using bioinformatical analysis. *Acta Epileptol.* **2**, 20 (2020).
39. Fritschy, J.-M. Epilepsy, E/I balance and GABA(A) receptor plasticity. *Front. Mol. Neurosci.* **1**, 5 (2008).
40. Prenosil, G. A. et al. Specific subtypes of GABAA receptors mediate phasic and tonic forms of inhibition in hippocampal pyramidal neurons. *J. Neurophysiol.* **96**, 846–857 (2006).
41. Pavlov, I. & Walker, M. C. Tonic GABA(A) receptor-mediated signalling in temporal lobe epilepsy. *Neuropharmacology* **69**, 55–61 (2013).
42. Koh, W., Kwak, H., Cheong, E. & Lee, C. J. GABA tone regulation and its cognitive functions in the brain. *Nat. Rev. Neurosci.* **24**, 523–539 (2023).
43. Samarut, É. et al. γ-Aminobutyric acid receptor alpha 1 subunit loss of function causes genetic generalized epilepsy by impairing inhibitory network neurodevelopment. *Epilepsia* **59**, 2061–2074 (2018).
44. Schweizer, C. The γ2 subunit of GABAA receptors is required for maintenance of receptors at mature synapses. *Mol. Cell. Neurosci.* **24**, 442–450 (2003).
45. Angelotti, T. & Macdonald, R. Assembly of GABAA receptor subunits: alpha 1 beta 1 and alpha 1 beta 1 gamma 2S subunits produce unique ion channels with dissimilar single- channel properties. *J. Neurosci.* **13**, 1429–1440 (1993).
46. Alldred, M. J., Mulder-Rosi, J., Lingenfelter, S. E., Chen, G. & Lüscher, B. Distinct γ2 subunit domains mediate clustering and synaptic function of postsynaptic $GABA_A$ receptors and gephyrin. *J. Neurosci.* **25**, 594–603 (2005).
47. Gataullina, S., Bienvenu, T., Nabbout, R., Huberfeld, G. & Dulac, O. Gene mutations in paediatric epilepsies cause NMDA-pathy, and phasic and tonic GABA-pathy. *Dev. Med. Child Neurol.* **61**, 891–898 (2019).
48. Scalise, S. et al. Generation of iPSC lines from two patients affected by febrile seizure due to inherited missense mutation in SCN1A gene. *Stem Cell Res.* **49**, 102083 (2020).
49. Parrotta, E. I. et al. Comprehensive proteogenomic analysis of human embryonic and induced pluripotent stem cells. *J. Cell. Mol. Med.* **23**, 5440–5453 (2019).
50. Mortazavi, A., Williams, B. A., McCue, K., Schaeffer, L. & Wold, B. Mapping and quantifying mammalian transcriptomes by RNA-Seq. *Nat. Methods* **5**, 621–628 (2008).
51. Liao, Y., Smyth, G. K. & Shi, W. featureCounts: an efficient general purpose program for assigning sequence reads to genomic features. *Bioinformatics* **30**, 923–930 (2014).
52. Love, M. I., Huber, W. & Anders, S. Moderated estimation of fold change and dispersion for RNA-seq data with DESeq2. *Genome Biol.* **15**, 550 (2014).
53. Ruffolo, G. et al. A novel action of lacosamide on GABAA currents sets the ground for a synergic interaction with levetiracetam in treatment of epilepsy. *Neurobiol. Dis.* **115**, 59–68 (2018).
54. Palma, E. et al. Microtransplantation of membranes from cultured cells to Xenopus oocytes: A method to study neurotransmitter receptors embedded in native lipids. *Proc. Natl. Acad. Sci.* **100**, 2896–2900 (2003).
55. Gaeta, A. et al. Membranes and synaptosomes used to investigate synaptic GABAergic currents in epileptic patients. *Membranes* **14**, 64 (2024).

Acknowledgements

The figures of this manuscript were created using BioRender. B.P. acknowledges Relatech S.p.A. for the partial funding of her doctoral fellowship.

Author contributions

EIP and GR conceived and supervised the study; S.S., Al.G., G.R., and E.I.P. planned and designed the experiments; S.S. and Al.G. performed most of the experiments; E.A., V.L., R.C., M.T., and L.J.L. performed some experiments; B.P., P.H.G., and P.V. performed the bioinformatic analysis; An.G. recruited the patients; S.S., Al.G., V.A., G.R., and E.I.P. performed analysis and interpretation of data; E.P., P.C., A.M., G.P., and G.C. provided critical discussions and expert perspectives to refine the research; S.S. and Al.G. prepared the figures and drafted the manuscript; G.R. and E.I.P. wrote the final version of the paper; E.P., P.C., G.R., G.C. and E.I.P. provided financial support. All authors read and approved the final manuscript.

Funding

The present study was funded by the Italian Ministry of University and Research through the following project: National Recovery and Resilience Plan (PNRR), Mission 4 "Education and Research" - Component C2, Investment 1.1, Fund for the National Research Program and Projects of National Relevant Interest (PRIN) 2022, project code 2022J2ARST to GR and EIP. This work was supported also by the Fondi Ateneo grants, grant nos. RM11916B84D24429 (EP), RG12117A8697DCF1 (EP, GR) funded by Sapienza University, AICE-FIRE 2022 (GR), PRIN 2022 (EP, GR and PC), PRIN-PNRR 2022 (EP) from the Italian Ministry of University and Research and PNC Project 0000001 "Digital Driven Diagnostics, Prognostics, and Therapeutics for Sustainable Healthcare", acronym D3 4 Health, funded by the Complementary Plan to PNRR and approved by Directorial Decree N. 1511 of September 30, 2022 to GC. GR was also supported by the Italian Ministry of Health, "Ricerca corrente". PC received the intramural grant from Department of Biotechnological and Applied Clinical Sciences of the University of L'Aquila: "DISCAB grant 2024", 07_DISCAB_grant_2024.

Declarations

Competing interests

The authors declare no competing interests.

Additional information

Supplementary Information The online version contains supplementary material available at https://doi.org/10.1038/s41598-025-09208-3.

Correspondence and requests for materials should be addressed to G.R.

Reprints and permissions information is available at www.nature.com/reprints.

Publisher's note Springer Nature remains neutral with regard to jurisdictional claims in published maps and institutional affiliations.